

pubs.acs.org/JPCB Article

# Understanding the Water-in-Salt to Salt-in-Water Characteristics across the Zinc Chloride: Water Phase Diagram

Shelby B. Pillai, Robert J. Wilcox, Berkley G. Hillis, Bradley P. Losey, and James D. Martin\*



Cite This: J. Phys. Chem. B 2022, 126, 2265-2278



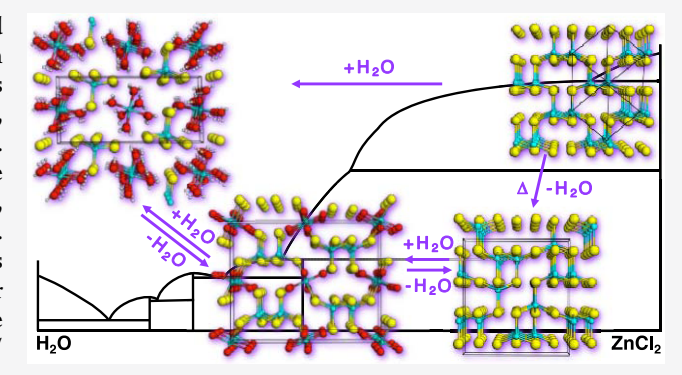
**ACCESS** 

Metrics & More

Article Recommendations

s Supporting Information

**ABSTRACT:** Using a series of time- and temperature-resolved synchrotron diffraction experiments, the relationship between multiple polymorphs of  $\operatorname{ZnCl_2}$  and its respective hydrates is established. The  $\delta$ -phase is found to be the pure anhydrous phase, while the  $\alpha$ ,  $\beta$ , and  $\gamma$  phases result from partial hydration. Diffraction, gravimetric, and calorimetric measurements across the entire  $\operatorname{ZnCl_2}$ : $\operatorname{R}$   $\operatorname{H_2O}$ ,  $\operatorname{O} > R > \infty$  composition range using ultrapure, doubly sublimed  $\operatorname{ZnCl_2}$  establish the  $\operatorname{ZnCl_2}$ :  $\operatorname{H_2O}$  phase diagram. The results are consistent with the existence of crystalline hydrates at R=1.33, 3, and 4.5 and identify a mechanistic pathway for hydration. All water is not removed from hydrated  $\operatorname{ZnCl_2}$  until the system is heated above its melting point. While hydration/dehydration is reversible in concentrated solutions, dehydration



from dilute aqueous solutions can result in loss of HCl, the source of hydroxide impurities commonly found in commercial  $ZnCl_2$  preparations. The strong interaction between  $ZnCl_2$  and water exerts a significant impact on the solvent water such that the system exhibits a deep eutectic at a composition of about R = 7 (87.5 mol %) and a eutectic temperature below -60 °C.

#### I. INTRODUCTION

Zinc chloride is one of the most soluble metal chloride salts, with a reported solubility of 437 g/100 g H<sub>2</sub>O (ZnCl<sub>2</sub>·R H<sub>2</sub>O, R = 1.73; 63 mol % H<sub>2</sub>O; 32 m) at 30 °C. For reference, at 30 °C, neighboring first-row transition metals exhibit saturation at R = 9.65 for CuCl<sub>2</sub>, R = 10.19 for NiCl<sub>2</sub>, and R = 12.07 for CoCl<sub>2</sub>. The origin of the extremely high solubility of ZnCl<sub>2</sub> is not clearly established, although it likely results from the formation of molecular ions whose size yields inefficient packing and thus ionic liquid formation. To characterize aqueous salt solubility, Braunstein proposed hydration categories of (I) Debye-Hückel limiting (100-99 mol % water), (II) extended Debye-Hückel (99-90 mol % water), (III) hydrate melts (90-75 mol % water), (IV) incomplete hydration sheaths (75-0.01 mol % water), and (V) gas solubility (<0.01 mol % water). Aqueous zinc chloride solutions remain liquid at room temperature across four of these five categories. Aqueous solutions of ZnCl<sub>2</sub> are widely applicable, with utility in electroplating,2 battery technology,3-5 solar energy conversion,6 formation and transport of hydrothermal ores, 7,8 and various biological functions. 9-12

Knowledge of the equilibrium  $\operatorname{ZnCl}_2: \operatorname{H}_2\operatorname{O}$  phase diagram is important to understand and apply structure/property relationships in such salt hydrate systems. Mylius and Dietz constructed the original  $\operatorname{ZnCl}_2: \operatorname{H}_2\operatorname{O}$  phase diagram, proposing the existence of crystalline hydrates at R=1.5, 2, 2.5, 3, and  $4^{13}$  (Braunstein's class III and IV hydrates). Although not observed in the original work, the R=1.33

hydrate phase was later crystallographically identified. <sup>14</sup> We previously characterized the crystalline and liquid structures of the R=3 hydrate. <sup>15–17</sup> Hennings et al. reported crystal structures of R=2.5 and 4.5 hydrates, <sup>18</sup> although neither were reported to be grown from their stoichiometric compositions. Our initial investigation of the phase diagram in the immediate vicinity of the congruently melting R=3 hydrate <sup>15</sup> shows a standard eutectic-type behavior with both  $H_2O$  and  $D_2O$  without evidence of a crystalline phase at composition R=2.5 (71% water). At the  $ZnCl_2$ -rich side of the phase diagram, four crystalline phases are reported  $(\alpha, \beta, \gamma, \text{ and } \delta)^{19-21}$  but there remains some debate as to which are truly anhydrous. <sup>22,23</sup>

Extensive measurements of concentration-dependent physical properties of the more dilute Braunstein class I–III aqueous solutions of ZnCl<sub>2</sub> have also been reported, such as activity, <sup>24–28</sup> conductivity, <sup>29–35</sup> vapor pressure, <sup>26,27,29</sup> density, <sup>30,31</sup> viscosity, <sup>31,33</sup> relaxation time for water exchange, <sup>36</sup> and glass-transition temperatures. <sup>32,37,38</sup> Anomalous behavior is frequently reported for multiple physical properties in class

Received: December 13, 2021 Revised: January 24, 2022 Published: February 10, 2022





II (extended Debye-Hückel) and class III (hydrate melt) regions of the ZnCl<sub>2</sub>: H<sub>2</sub>O system.

It has been suggested that polymeric chains in concentrated solutions and glasses may be responsible for the anomalous behavior in the  $\rm ZnCl_2: H_2O$  system. <sup>38,39</sup> However, our discovery of the ionic liquid nature of the R=3 system <sup>15–17</sup> leads us to suggest that a series of hydration shells rather than polymeric chains may be responsible for the anomalous reported concentration-dependent properties. Both computational and experimental reports establish the first hydration shell in aqueous zinc salts to be  $[\rm Zn(OH_2)_6]^{2+}$ . <sup>40–43</sup> Beyond the highly polarized first hydration shell, multiple reports suggest the existence of a more weakly polarized second hydration shell. <sup>41,44–47</sup>

As part of our ongoing research to understand structure transformations in condensed matter between liquid and solid systems, we here report a rigorous characterization of the equilibrium ZnCl<sub>2</sub>: H<sub>2</sub>O phase diagram. This work was carried out using ultrapure, doubly sublimed ZnCl2 to avoid inconsistencies introduced by ubiquitous hydroxide impurities found in many commercially available sources of "anhydrous" zinc chloride. Using temperature-/time-resolved synchrotron diffraction (TtXRD), we demonstrate that the presence of water is responsible for the multiple polymorphs of crystalline ZnCl<sub>2</sub>. By TtXRD and thermogravimetric analysis (TGA), we demonstrate structural hysteresis of the hydration process. These measurements, along with differential scanning calorimetry (DSC) and variable-temperature (VT) synchrotron and neutron diffraction, are used to differentiate kinetic and thermodynamically stable phases such that a more accurate equilibrium phase diagram is established.

Herein, the results (Section III) are presented with a systematic hierarchy of techniques: Section III.I diffraction, Section III.III gravimetric analysis, Section III.III calorimetry, then composition: solution characteristics are best described by dividing Braunstein's five classes of hydrates into three groupings, including Section III.III.I ZnCl<sub>2</sub>-rich (classes V and IV), Section III.III.III stoichiometric hydrates (class III), and Section III.III.III water-rich (classes II and I). The compilation of all results is then discussed (Section IV) with respect to Section IV.I the ZnCl<sub>2</sub>: H<sub>2</sub>O phase diagram, Section IV.II how water influences the polymorphs of crystalline ZnCl<sub>2</sub>, and Section IV.III mechanistic insight into the hydration process.

#### II. EXPERIMENTAL METHODS

II.I. Materials and Synthesis. Zinc chloride (Aldrich) was sublimed under dynamic vacuum across a gradient from 350 °C to room temperature. The sublimed product was harvested in a nitrogen-filled glovebox, sealed under vacuum into a 2 cm  $\times$  30 cm Pyrex tube, and sublimed a second time under static vacuum at 330 °C. Powder X-ray diffraction (XRD) and DSC analysis confirmed the sublimed material to be anhydrous δ-ZnCl<sub>2</sub> (mp 318 °C). The purified zinc chloride was stored in a glovebox under a dry nitrogen atmosphere.

All solutions were made with 18  $M\Omega$  water ( $H_2O$ ) obtained from a Millipore Synergy ultrapure water filtration system or with as purchased 99.99%  $D_2O$  (Aldrich).

Samples for ex situ bulk hydration were made by placing ultrapure, doubly sublimed  $\delta$ -ZnCl<sub>2</sub> into glass vials. The desired stoichiometric amount of water was pipetted into each vial. The capped samples were stored at room temperature and periodically agitated over 2–4 days before further measurements were taken.

II.II. Differential Scanning Calorimetry (DSC). DSC measurements (TA Instruments Q250 or Q2000) were conducted on aqueous zinc chloride solutions over composition ranges of  $0.01 \le R \le 500 \ (1-99.8 \ \text{mol} \ \% \ \text{water})$  with  $H_2O$ , and  $2.6 \le R \le 3.6 \ (72-78 \ \text{mol} \ \% \ \text{water})$  with  $D_2O$ . In a typical run, a sample was placed into the DSC at 35 °C and cycled through cooling and heating profiles from −50 or −80 to 25 or 50 °C for water-rich samples, and from 0 or 25 to 200 or 325 °C for zinc chloride-rich samples, at 0.5, 1.0, 3, 5 or 10 °C/min. For the purposes of characterizing the phase diagram, eutectic and liquidus temperatures are identified as the maximum of the peak in the DSC traces, which are then corrected with respect to the instrumental response for which the peak maximum lags the onset, about 2 °C, depending on the heat/cool rate of the experiment.

DSC samples were prepared in a nitrogen-filled glovebox or in air as bulk samples from which a 20-40 mg aliquot was extracted, or about 20 mg of doubly sublimed  $\delta$ -ZnCl $_2$  and the appropriate amount of water (H2O or D2O) were combined, and then placed in a high-pressure stainless steel DSC pan which was then hermetically sealed with a gold seal. Additional samples were prepared by placing a measured amount of  $\delta$ -ZnCl<sub>2</sub> into a high-pressure stainless steel DSC pan on the stage of a home-built environmentally controlled microbalance (microbalance head from CI Electronics, controlled by LabWeigh Software). A stream of nitrogen was hydrated by bubbling through water, which was then passed over the sample until the desired stoichiometric amount of water was sorbed. From these samples,  $1-2 \text{ mm} \times 0.7 \text{ mm}$  aliquots were removed, and flame sealed into 0.7 mm ID fused silica capillaries. The remaining material was hermetically sealed into the DSC pan with a gold seal to obtain a set of equivalent samples for DSC and subsequent diffraction measurements, ensuring equivalent composition for structural and calorimetric analysis.

**II.III.** Thermogravimetric Analysis (TGA). TGA measurements (TA Instruments Q50) were conducted by placing anhydrous  $\delta$ -ZnCl<sub>2</sub> in a ceramic sample cup over which a carrier gas was passed. For the dry purge flow stream, nitrogen was dried by passing through a 50 cm column of solid NaOH. The sample chamber was initially equilibrated at 31 °C. The purge gas stream was then switched to moist nitrogen with a 4.6 Torr vapor pressure of water, controlled by bubbling nitrogen through water equilibrated at 0 °C. After 7–8 h of sorption, the moist nitrogen stream was switched to dry nitrogen to dehydrate the sample, followed by heating to an isotherm of 120 °C or ramping from 31 to 360 °C.

Additional gravimetric measurements were conducted using our home-built environmentally controlled microbalance with equivalent streams of dried or moist nitrogen (Water vapor pressure:  $P_{\rm H_2O}$  = 4.6 Torr). For these experiments, anhydrous  $\delta$ -ZnCl<sub>2</sub> was placed on a glass coverslip on the microbalance stirrup with the carrier gas passed directly over the sample. The sample temperature was controlled to isotherms between 5 and 90 °C.

II.IV. Time-/Temperature-Resolved X-ray Diffraction (TtXRD). The hydration and dehydration of ZnCl<sub>2</sub> were investigated using a translating image plate (TIP) detector on the beamline X7B at the National Synchrotron Light Source (NSLS), Brookhaven National Laboratory. The TtXRD experimental design was analogous to that previously reported for the study of ethylene sorption into CuAlCl<sub>4</sub>. A powdered

sample of  $\delta$ -ZnCl<sub>2</sub> was loosely packed into a 0.7 mm ID fused silica capillary between plugs of glass wool. The open-ended capillary was placed into a 1.0 mm ID sapphire capillary which was connected via Swagelok fittings to a goniometer-mounted, electronically controlled gas manifold to switch between vacuum, dry nitrogen, and moist nitrogen (5–10 cm³/min), saturated by bubbling through water at room temperature ( $P_{\rm H_2O} \sim 20$  Torr). Using a Debye–Scherrer collection geometry, the TIP detector provided 30–40 s time resolution by exposing a radial slice of the full Debye–Scherrer rings through a slit in a plate that translates across 20 cm × 40 cm image plate. The capillary sample was not rotated during the data collection. This method is particularly susceptible to preferred orientation effects since crystallite size, orientation, and distribution may change during the course of the reaction.

To evaluate the thermal dehydration/rehydration, a sample of the  $R=1.33~{\rm ZnCl_2}$  hydrate was made by exposing  $\delta\text{-ZnCl_2}$  to moist air at ambient temperature until it became a fully liquid droplet. Upon subsequent exposure to cool dry air, the droplet became a slurry. This mostly solid slurry was packed between plugs of glass wool into a 0.7 mm ID fused silica capillary. The sample was mounted on the gas-manifold goniometer, and diffraction data were collected while heating from room temperature (~20 °C) to 325 °C at 3 °/min using a nichrome wire heater adjacent to the sample capillary. The sample was then cooled to room temperature at a rate of 5 °/min. Equivalent dehydration experiments were conducted with the sample under autogenous pressure with the gas manifold closed and with the sample under dynamic vacuum.

**II.V.** *Ex Situ* X-ray Diffraction. For phase identification of the zinc chloride polymorphs as a function of water exposure, a powdered or slurry sample with between 1 and 45 mol % water was placed on cellophane tape and rolled into a reasonably airtight tube that was affixed to a brass pin mounted on a goniometer. Diffraction data were collected using a Rigaku R-Axis Spider diffractometer with Cu K $\alpha$  ( $\lambda$  = 1.541 Å) in a Debye–Scherrer geometry (transmission mode) with a curved image plate detector.

II.VI. Neutron Diffraction. Each of the aqueous zinc chloride solutions (0.5 mL) for 23 compositions ranging from R=3 to 250 (75.0–99.6 mol % water) was sealed into 5 mm OD fused silica NMR tubes (WILMAD). These and an empty NMR tube were mounted on the linear sample changer on a NOMAD diffractometer, Spallation Neutron Source, Oak Ridge National Lab. The linear sample changer was equipped with an Oxford Cobra Plus Cryosystem using an Ar gas stream. Total scattering data were collected to  $Q_{\rm max}=50~{\rm \AA}^{-1}$  and calibrated with respect to a diamond powder standard. Room-temperature data were collected for all compositions. Variable-temperature data were collected for the R=3, 4, 9, 21, and pure  $D_2O$  compositions at specific isotherms between 100 and 333 K (sum of three 20 min scans) or with a ramped temperature profile 1 or 5 °/min.

### III. RESULTS

A detailed description of the results required to characterize the full  $ZnCl_2: H_2O$  phase diagram and to understand both kinetic and thermodynamic phase transformations is provided in the Supporting Information. However, to enhance manuscript readability and publication page economy, we here provide only a summary of the most germane results. Hereafter, all figures presented in the main text are indicated

numerically, and those in the Supporting Information are indicated as Figure SX.

III.I. Crystalline Structures of Zinc Chloride and Its Hydrates. III.I.I. Zinc Chloride-Rich Compositions: Incomplete Hydration Sheaths and Gas Solubility (Hydrate Classes IV and V).  $ZnCl_2$  is highly hygroscopic; at ambient temperature, we have observed sorption of up to 21 equiv of water from the atmosphere. To examine the correlation between water vapor exposure and the various reported polymorphs and hydrates of  $ZnCl_2$ , a series of TtXRD measurements were performed during both hydration of doubly sublimed, anhydrous  $\delta$ - $ZnCl_2$  and and dehydration/rehydration of the crystalline  $ZnCl_2 \cdot 1.33$  H<sub>2</sub>O hydrate phase (57 mol % water).

The time-resolved diffraction data for the ambient-temperature, *in situ* hydration of doubly sublimed, anhydrous  $\delta$ -ZnCl<sub>2</sub> are shown in Figure 1. Upon exposure to water vapor-saturated

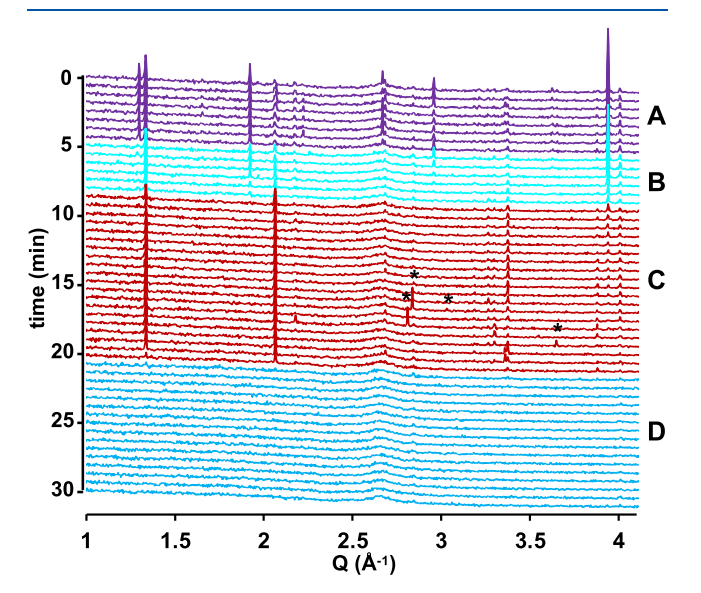


**Figure 1.** Time-resolved synchrotron diffraction of the ambient-temperature hydration of  $\delta$ -ZnCl<sub>2</sub>. (A) Starting material is  $\delta$ -ZnCl<sub>2</sub> (purple) under dry nitrogen. (B) A mixture of  $\delta$ -ZnCl<sub>2</sub> and  $\alpha$ -ZnCl<sub>2</sub> (turquoise) is observed immediately upon exposure to water vapor-saturated nitrogen at 4.5 min. (C) Upon further exposure to water vapor, the material becomes predominantly  $\alpha$ -ZnCl<sub>2</sub> (red), before (D) forming a hydrated melt (blue). Asterisks (\*) represent transient diffraction peaks consistent with  $\beta$ -ZnCl<sub>2</sub>.

nitrogen ( $P_{\rm H_2O} \sim 20$  Torr), the anhydrous  $\delta$ -ZnCl<sub>2</sub> transforms to the  $\alpha$ -phase before forming an amorphous solution/melt. While a few transient peaks between  $Q = 2.5-3.5 ~\rm \AA^{-1}$  can be indexed to the  $\beta$  phase, there is no evidence for the formation of either the  $\gamma$  polymorph, nor the R = 1.33 hydrate, the most water-deficient class IV hydrate.

Partially dehydrating the ambient-temperature water-saturated liquid produces a slurry. By diffraction, the only crystalline phase is the R=1.33 hydrate (Figure 2A, dark blue). To observe the thermal dehydration/hydration behavior, this slurry was heated from room temperature to 325 °C and then cooled to room temperature in a closed system while collecting the *in situ* TtXRD, Figure 2. Here, the full manifold volume was significantly larger than the capillary, preventing significant autogenous pressure upon water desorption.

Upon heating, the diffraction peak characteristics of the R = 1.33 hydrate disappear around 40 °C, while those correspond-

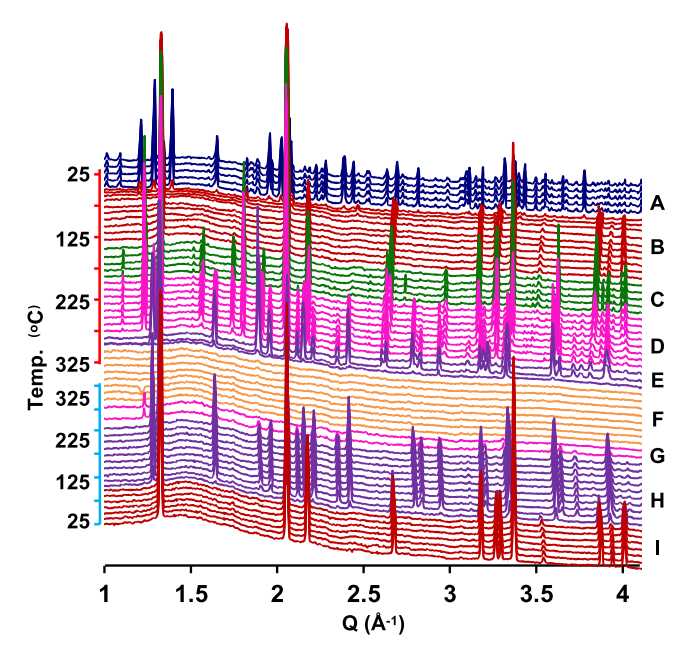


**Figure 2.** Temperature-/time-resolved diffraction of a sample of ZnCl<sub>2</sub>·1.33 H<sub>2</sub>O in a closed capillary/gas-manifold system that was heated at 3 °/min from ~2 to 325 °C, held at 325 °C for about 5 min, then cooled to room temperature at 5 °/min. (A) ZnCl<sub>2</sub>·1.33 H<sub>2</sub>O (dark blue); (B)  $\alpha$ -ZnCl<sub>2</sub> (red); (C)  $\beta$ -ZnCl<sub>2</sub> (green); (D) mixture of  $\beta$ -ZnCl<sub>2</sub> and  $\delta$ -ZnCl<sub>2</sub> (fuchsia); (E)  $\delta$ -ZnCl<sub>2</sub> (purple); (F) melt (yellow); (G)  $\beta$ -ZnCl<sub>2</sub> and  $\delta$ -ZnCl<sub>2</sub> (fuchsia); (H)  $\delta$ -ZnCl<sub>2</sub> (purple); and (I)  $\alpha$ -ZnCl<sub>2</sub> (red).

ing to  $\alpha$ -ZnCl<sub>2</sub> grow in. The  $\alpha$ -ZnCl<sub>2</sub> experiences noticeable changes in lattice constants (Figure S1) before transforming to  $\beta$ -ZnCl<sub>2</sub> around 150–160 °C. The  $\beta$ -phase persists through the region Figure 2C (green) until the  $\delta$ -phase begins to appear at about 200 °C. Both  $\beta$  and  $\delta$  phases coexist to about 280 °C (region Figure 2D, fuchsia). The  $\delta$ -phase is the last crystalline phase observed before zinc chloride melts between 300 and 310 °C, region Figure 2E (purple). Pure, anhydrous  $\delta$ -ZnCl<sub>2</sub> melts at 318 °C, but it is likely that the presence of moisture in the closed gas manifold depresses the melting point. Upon supercooling from the melt, the  $\beta$ -phase is the first phase to nucleate, but soon transforms to  $\delta$ -ZnCl<sub>2</sub>, regions Figure 2G,H. Subsequent isothermal crystallization measurements using doubly sublimed ZnCl<sub>2</sub> also have demonstrated kinetic formation of the  $\beta$ -phase with subsequent trans-

formation into the thermodynamically favored  $\delta$ -phase. Around 100 °C, the sample abruptly converts from  $\delta$ -ZnCl<sub>2</sub> (region Figure 2H) to  $\alpha$ -ZnCl<sub>2</sub> (region Figure 2I), analogous to the water vapor-induced  $\delta$ -to- $\alpha$  transition in Figure 1. Residual water trapped in the closed gas manifold induces this transformation.

A similar dehydration of the R=1.33 hydrate TtXRD experiment was conducted under dynamic vacuum to remove any residual water vapor (Figure S2). With the removal of excess water vapor, the 1.33 hydrate first transforms into a poorly crystalline  $\beta$ -phase, then a combination of liquid and increasingly crystalline  $\beta$ -phase. The fully crystalline  $\beta$ -ZnCl<sub>2</sub> transforms to the  $\delta$ -phase between 200 and 250 °C. Under dynamic vacuum, the system melts at about 315 °C. The  $\delta$ -phase is both the melting and recrystallizing phase.

Complementary powder XRD of bulk samples hydrated ex situ by the addition of liquid water to pure anhydrous  $\delta$ -ZnCl<sub>2</sub> shows complex time-dependent phase behavior. Compositions with 1–10 mol % water initially exhibit the  $\gamma$ -ZnCl<sub>2</sub> structure (Figure S3a) but transform to  $\alpha$ -ZnCl<sub>2</sub> upon melting and recrystallizing. Samples with 15–30 mol % water initially consist of  $\gamma$ -ZnCl<sub>2</sub> then partially transform to the 1.33 hydrate over time. Single crystals extracted from multiple room-temperature saturated solutions all exhibit  $\alpha$ -ZnCl<sub>2</sub> single-crystal diffraction patterns.

III.I.II. Variable-Temperature Diffraction for Hydrate Classes II and III. Having investigated the phase behavior upon adding small amounts of water to zinc chloride, it remains to identify the phase behavior of water-rich compositions. To do this, a series of variable-temperature (VT) neutron diffraction measurements were conducted for R = 3, 4, 9, and 21 compositions, and pure  $D_2O$ . Previous synchrotron diffraction work on compositions between 2.5 < R < 3.5 only showed evidence of the crystalline R = 3 hydrate, [Zn(OH<sub>2</sub>)<sub>6</sub>][ZnCl<sub>4</sub>]. Figure S4 shows the low-temperature neutron diffractograms. No crystallization was observed for the R = 4 or 9 compositions. The R = 21 neutron diffraction pattern can be indexed to crystalline ice; no other crystalline phases were observed. It must be noted that particularly throughout the class III hydrate region (R = 3-9, 75–90 mol % water), glasses readily form. Thus, the absence of observed crystalline hydrates at certain compositions may be because none exist, or it may be that nucleation does not occur under the conditions explored. We suspect the latter, as subsequent observation of crystallization by polarized light optical

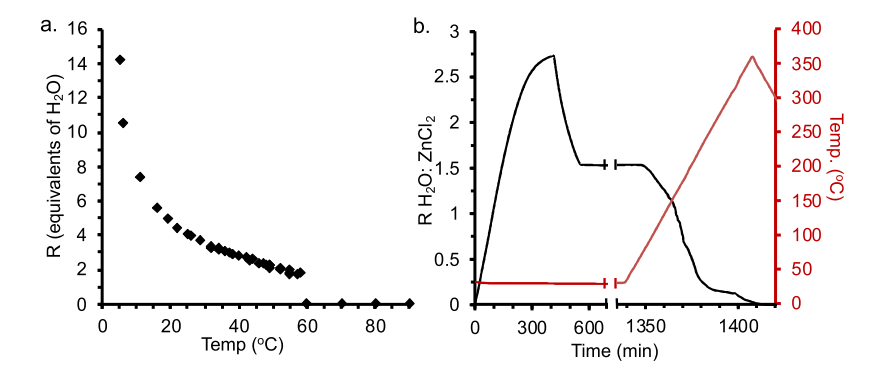


**Figure 3.** Thermogravimetric hydration/dehydration of ZnCl<sub>2</sub>. (a) Equilibrium sorption isotherm data for the hydration of ZnCl<sub>2</sub> under a water partial pressure of 4.6 Torr. (b) Hydration of ZnCl<sub>2</sub> at 31  $^{\circ}$ C and  $P_{H_2O}$  = 4.6 Torr, and subsequent dehydration under dry nitrogen followed by heating at 5.0  $^{\circ}$ /min to 360  $^{\circ}$ C.

microscopy (POM) of a thin film of sample between a microscope slide and coverslip, reveals two types of crystals with distinct morphologies consistent with the existence of a second crystalline phase, likely the R = 4.5 hydrate, between the R = 3 hydrate and water-ice (Figure S5).

**III.II.** Thermogravimetric Analysis of Zinc Chloride Hydrate Formation. In complementary experiments, the hydration/dehydration of  $ZnCl_2$  was examined by thermogravimetric analysis. The extent of water sorption depends on the temperature of the experiment and the relative water vapor pressure. For example, as shown (Figure 3a) in the sorption experiments with  $P_{H_2O} = 4.6$  Torr, no water sorption by  $\delta$ -  $ZnCl_2$  is observed for sample temperatures above 60 °C. At 58 °C, the hydrate composition equilibrates to R = 1.7, increasing to R = 14.3 at 5 °C.

All gravimetric sorption experiments exhibit a smooth, monotonic increase in the extent of hydration until the equilibrium concentration is achieved. 16 No gravimetric experiments have provided any evidence for the formation of the R = 1.33 hydrate upon sorption of water into  $ZnCl_2$ ; the 1.33 hydrate was only observed for bulk samples under conditions with stoichiometric or substoichiometric amounts of water in samples that equilibrated for about a week. However, equilibrium compositions consistent with the 1.33 hydrate and lower extents of hydration are observed gravimetrically upon dehydration of more water-rich ionic liquid compositions under dry nitrogen and with heating, as reported in Figures 3b and S6. At 31 °C under dry nitrogen, the hydrated samples equilibrate to an R = 1.5 composition that consists of a slurry of the R = 1.33 crystalline phase and a more water-rich solution. The first derivative of the weight loss vs time for further heating to an isotherm of 120 °C or by a ramp to 360 °C (Figure S6), shows additional water is lost in a stepwise manner. Remarkably, the last 0.1 equiv of water only begin to desorb at 310 °C and are not fully lost until 350 °C, well after the sample has melted.

It is worthwhile to note that the reversibility of the hydration/dehydration observed in the above diffraction and TGA experiments contrasts the many textbook reports suggesting HCl is lost upon evaporation of aqueous zinc chloride solutions, forming mixed Zn(Cl/OH)<sub>2</sub> species. We find that bulk recovery of ZnCl<sub>2</sub> from dilute aqueous solutions under vacuum using a rotary evaporator is distinct from the results of TGA desorption of a concentrated solution at ambient pressure under a stream of dry nitrogen. Distilling water off an R = 100 solution at 70 °C with the condenser cooled to -15 °C yields a residual liquid with between 3 and 4 equiv of water per ZnCl<sub>2</sub>. Placing this residual liquid into an oven at 110 °C removes additional water, leaving a mixture of about 10% crystalline material and 90% hydrate melt. Upon cooling to room temperature, about 40% crystalline product is formed. Single-crystal unit cell determination by X-ray diffraction indicates the crystals grown at 110 °C and upon cooling to room temperature both are  $\alpha$ -ZnCl<sub>2</sub>. Re-dilution of the residual hydrate melt reveals a small amount of an insoluble precipitate which is identified by XRD powder diffraction to be the hydroxide/chloride, Zn<sub>5</sub>Cl<sub>2</sub>(OH)<sub>8</sub>·H<sub>2</sub>O (the mineral simonkolleite). This product, resulting from the loss of HCl upon heating under vacuum, is a common impurity in many commercially available zinc chloride products, often present at 1-2 wt %.

III.III. Calorimetry of Zinc Chloride Hydrates. DSC heating/cooling measurements of the zinc chloride hydrates provide additional insight into the complex phase behavior of this system. Similar to the melt/crystallization behavior of halite brines<sup>52</sup> and silicate magmas,<sup>53</sup> the presence of water significantly influences the thermochemistry in the zinc chloride/water system. Thus, for this study, all measurements were conducted in high-pressure stainless steel DSC pans to ensure no water loss from the system occurs upon heating. The calorimetry of this system is best understood across three distinct compositional regions including the gas solubility and incomplete hydration sheaths (0-55 mol % water, Hydrate Classes IV and V), the hydrate melts (55-87 mol % water, Hydrate Class III), and the Debye-Hückel limiting and extended Debye-Hückel solutions (87-100 mol % water, Hydrate Classes I and II).

III.III.I Incomplete Hydration Sheaths and Gas Solubility (Hydrate Classes IV and V). DSC heating/cooling measurements of the bulk prepared samples with 1–55 mol % water reveal a complex mixture of structural phase transitions along with the sorption/desorption of water. A detailed description of the concentration-dependent calorimetry is provided in the Supporting Information, including representative calorimetry traces in Figure S7. The first heat exhibits extremely irregular behavior indicating the inhomogeneity of hydration among different grains of the as-prepared samples, consistent with the sample history dependence seen in the diffraction results reported above. Subsequent heating/cooling cycles exhibit regular and repeatable thermal transitions.

Thermal events likely associated with the peritectic decomposition of the R=1.33 hydrate are observed at irregular temperatures, and only for the more water-rich compositions, likely due to sample heterogeneity. Two small endotherms are normally observed at around 105 and 212  $^{\circ}$ C, consistent with certain water-loss and structural transitions also observed by gravimetric and diffraction measurements. A slow, persistent endothermic heat evolution consistent with the more gradual water loss is observed beyond the 105  $^{\circ}$ C endotherm, reaching a maximum at what appears to be the liquidus.

The 1 mol % water sample exhibits a sharp liquidus transition at 316 °C, a temperature just slightly below that of pure, anhydrous  $\delta$ -ZnCl<sub>2</sub>. Notably, the magnitude of this endotherm (8.91 kJ/mol) is slightly larger than for melting pure anhydrous  $\delta$ -ZnCl<sub>2</sub> (318 °C, 8.76 kJ/mol) consistent with it being a combination of melting and loss of water. The liquidus peak shifts to a systematically lower temperature with increasing water content (to 276 °C for 10 mol % water). The integrated area of the liquidus peak systematically diminishes with added water, with a trend that extrapolates to zero at 13-14 mol % water. Notably, no corresponding endotherm is observed in the 15 mol % sample. Instead, new endothermic features are observed that shift to higher temperature reaching a maximum at about 312 °C for the 20 mol % water composition. With increasing amounts of water, the lowest of these endothermic features shifts to a lower temperature exhibiting a more conventional liquidus-type trend. However, visually, samples sealed in capillaries and heated in a box furnace exhibit melting over a large range of temperatures but are fully liquid at temperatures below these DSC observed endotherms (compare Figures S7 and S8). The highertemperature endotherms above 300 °C are likely a result of loss of water upon heating, which is also observed by bubble evolution upon melting of samples in capillaries.

III.III.II. Hydrate Melts (Hydrate Class III). The original Mylius—Deitz phase diagram identifies multiple hydrate phases between the compositions of  $1.5 \le R \le 4.0$  (60–80 mol % water). However, their data in this region are complex and not internally consistent; potentially a result of the common  $\rm Zn_5Cl_2(OH)_8$ ·H<sub>2</sub>O impurity. Figure S9 compares the original Mylius—Deitz data with our current data. Systematic DSC experiments over this concentration range using ultrapure, doubly sublimed  $\rm ZnCl_2$  and ultrapure water (18 M $\Omega$  H<sub>2</sub>O or as purchased 99.999% D<sub>2</sub>O (Aldrich)) clarify the existence and/or the thermodynamic phase stability of the respective zinc chloride hydrate phases.

The calorimetry of the 58-65 mol % water compositions  $(1.38 \le R \le 1.86)$  generally exhibit an endotherm at about 22 °C. This endotherm is frequently broadened, at times presenting with a double maximum. This feature is consistent with the presence of both a peritectic defining the upper temperature of stability for the R = 1.33 hydrate, and the water-loss that leads to the R = 1.5 composition observed via TGA (Figures 3 and S6).

The DSC heating data demonstrate classic eutectic behavior between 65 and 75 mol % water,  $1.9 \ge R \ge 3$ . Representative examples of DSC heating scans are shown in Figure S10. Single melting exotherms are observed both at the eutectic composition at 70 mol % water, R=2.3, and at the congruently melting 75 mol %, R=3 hydrate. At intermediate compositions, the relatively invariant endotherms observed at about -1 °C for  $H_2O$  and about -7 °C for  $D_2O$ , identify the eutectic temperature. By contrast, the liquidus temperature is composition-dependent, rising to a maximum at the congruently melting composition of the R=3 hydrate and to the peritectic near R=1.5. The congruently melting R=3 hydrate melts at 4.8 °C (13.7 kJ/mol) for  $H_2O$  and at -3.0 °C (11.4 kJ/mol) for  $D_2O$ .

Compositions between 75 and 83 mol % water (3 < R < 5)for this aqueous zinc chloride system also exhibit classic eutectic behavior and should be considered hydrate melts (Figure S11). By integrating the magnitude of the eutectic and liquidus endotherms and using the lever rule, it is possible to establish a eutectic composition at  $R \sim 4.1$  (80.4 mol %), equivalently observed for both the H2O and D2O data. This eutectic temperature is observed at -32 °C for  $H_2O$  and -37for D2O. A eutectic endotherm is not observed for compositions R > 4.1. However, the shape of the melting endotherm for the R = 4.65 composition in Figure S11a is noticeably broadened to lower temperature, indicative of a liquidus, rather than a eutectic feature. This, combined with the POM images (Figure S5) that show the growth of crystals with two distinct morphologies for compositions between R =3 and 4 when cooled to below  $T_{\text{eut}}$  provides thermodynamic evidence that is consistent with the crystalline R = 4.5 hydrate, reported by Hennings.18

III.III.III. Debye—Hückel Limiting and Extended Debye—Hückel Solutions (Hydrate Classes I and II). There is a substantial region between about  $5 \ge R \ge 7$  (80 to 87.5 mol % water) where we observe no crystallization, even in samples cooled in the DSC to -80 °C, or more rapidly quenched into liquid nitrogen. The Mylius—Deitz phase diagram does report some liquidus transitions in this region, <sup>13</sup> Figure S9, though again, we cannot rule out the possibility that this may be a result of hydroxide impurities in their ZnCl<sub>2</sub>.

Water-ice liquidus transitions are observed for compositions with R > 7 in DSC heating traces (Figure S12), first appearing in the R = 7.85 composition. Lever rule analysis based on the integrated heat flow suggests a eutectic composition between 85 and 87 mol % water, about R = 6. However, no signatures of the eutectic temperature were observed in any experiments down to  $-80~^{\circ}\text{C}$  by DSC or to  $-173~^{\circ}\text{C}$  by neutron diffraction.

#### IV. DISCUSSION

**IV.I.**  $ZnCl_2: H_2O$  **Phase Diagram.** Compiling the above temperature/composition data from diffraction, calorimetry, and gravimetric measurements leads to a more accurate  $ZnCl_2: H_2O$  phase diagram (Figure 4) than that originally presented

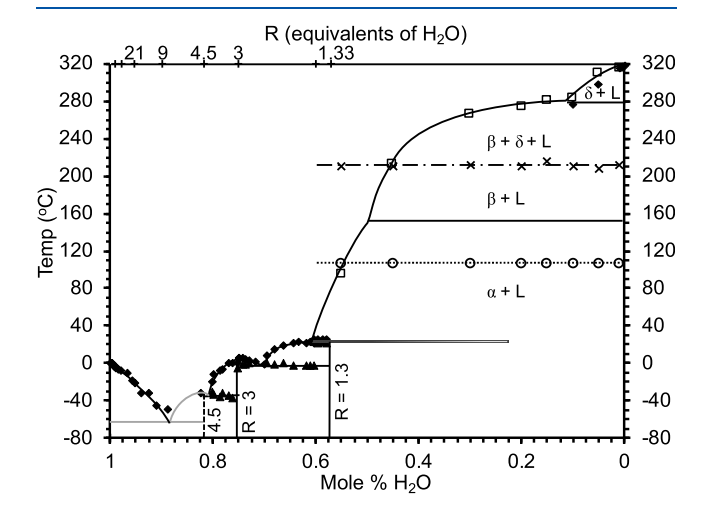


**Figure 4.** Temperature composition phase diagram for the  $ZnCl_2$ :  $H_2O$  system. Liquidus transitions are represented by filled diamonds (DSC) and open squares (visual melt in sealed capillaries). Eutectic/peritectic transitions are represented by filled triangles (DSC). Open circles/dotted line and  $\times$  symbols/dot-dashed line represent small transitions in the DSC that appear to correspond to the onset of water loss (TGA).

by Mylius and Dietz.<sup>13</sup> The additional measurements reported here are consistent with our previous publication of the hydrate class III-IV portion of the phase diagram for both H<sub>2</sub>O and D<sub>2</sub>O.<sup>15</sup> We propose the significant differences between the present work and that of earlier reports is largely a result of our use of ultrapure, doubly sublimed ZnCl<sub>2</sub>, as opposed to preparations that may have residual hydroxide impurities. This is most evident by comparison of the reported melting points of ZnCl<sub>2</sub>. Pure, anhydrous  $\delta$ -ZnCl<sub>2</sub> melts at 318 °C. The addition of 10 mol % (2.7 wt %) water depresses the melting point to 290 °C. But the moisture content cannot account for the extremely low melting point of 262 °C reported by Mylius and Dietz. 13 By contrast, DSC measurement of a commercial sample sold as ">98% extra pure ZnCl<sub>2</sub>", which was found to contain about 2 wt % Zn<sub>5</sub>Cl<sub>2</sub>(OH)<sub>8</sub>·H<sub>2</sub>O, exhibits a sharp melting transition at 284 °C. The substantial variation in reported melting points is likely due to hydroxide

It is important to recognize that composition/temperature phase diagrams, such as those presented here, make the assumption of isobaric conditions. However, analogous to other brine systems, 52 this system is not isobaric at elevated temperatures where the solution composition of the ZnCl<sub>2</sub>:

H<sub>2</sub>O system is highly dependent on the water vapor pressure. The effect of water vapor pressure is particularly evident for compositions with less than 60 mol % water and at elevated temperature, for which observed phase characteristics vary significantly depending on the head-space and/or any temperature gradients in the sample container. The added vapor pressure degree of freedom, according to the Gibbs phase rule, also allows for the coexistence of three phases in regions of temperature composition space, a condition only possible at a univariant point in a conventional composition/ temperature binary phase diagram. In Figure 4, the transitions most significantly affected by the water vapor pressure are marked by dashed lines. The temperature-phase-composition characteristics of the ZnCl<sub>2</sub> : H<sub>2</sub>O system below room temperature and with greater than 60 mol % water can be reasonably described as a conventional isobaric binary phase diagram. At higher temperatures and lower amounts of water, multiple thermal events are identified as a combination of structural and compositional phase transitions. Nevertheless, the pseudo-isobaric phase diagram of Figure 4 can be useful to practically understand the overall phase stability of the system, discussed below according to the logical groupings of hydrate classes.

*IV.I.I.* Incomplete Hydration Sheaths and Gas Solubility (Hydrate Classes IV and V). Incorporating small amounts of water into crystalline  $\rm ZnCl_2$  results in extensive polymorphism of ostensibly pure  $\rm ZnCl_2$  phases, which are actually various gashydrate phases as discussed in Section IV.II. DSC (Figure S7) data demonstrate that the addition of up to 13–14 mol % water to  $\delta$ -ZnCl<sub>2</sub> depresses the liquidus from 318 to 280 °C. There is a substantial flattening of the composition/temperature slope of the liquidus with greater than 15 mol % water where the gas-hydrate  $\beta$ -ZnCl<sub>2</sub> becomes the melting/crystallizing phase. An additional change in the liquidus slope occurs at approximately 50 mol % water and 150 °C beyond which  $\alpha$ -ZnCl<sub>2</sub> becomes the melting/crystallizing phase.

IV.I.II. Stoichiometric Hydrates (Hydrate Class III). The R=1.33 hydrate is the first observed stoichiometric hydrate and the only one observed as a crystalline solid at room temperature and ambient pressure. The crystalline R=1.33 hydrate is an incongruently melting phase, decomposing to a mixture of  $\alpha$ -ZnCl<sub>2</sub> and solution. The peritectic decomposition temperature is observed to be near room temperature, although it appears to shift toward higher temperatures for more water-deficient compositions in hermetically sealed DSC pans, wherein significant autogenous water vapor pressure is generated. This peritectic becomes largely nonobservable with less than 25 mol % water, with no clear boundary features identifying the limits of gas-hydrate solid solubility. Thus, this peritectic is represented as a fading line on the phase diagram (Figure 4).

We do not observe data consistent with the existence of an R = 1.5 crystalline hydrate (60 mol % water) as suggested in the original phase diagram. The R = 1.33 hydrate may have been originally interpreted as the 1.5 hydrate. The TGA desorption experiments at 31 °C under dry nitrogen exhibit a plateau at R = 1.5 (Figures 3 and S6), providing possible evidence for an R = 1.5 composition, but at the measured 31 °C isotherm, this composition is a slurry. Furthermore, the magnitude of the equilibrium isotherm is dependent on the temperature (Figure 3) as well as on the  $P_{\text{H-O}}$ . The other potential evidence for a

crystalline 1.5 hydrate is that the eutectic with the R=3 hydrate is first observed by DSC at about 60 mol % water (R=1.5). However, the only equilibrium crystalline phases observed between  $1.33 \ge R \ge 3$  have been the R=1.33 hydrate, the R=3 hydrate, and  $\alpha$ -ZnCl<sub>2</sub>. Together, these data suggest that there is no equilibrium 1.5 crystalline hydrate phase.

Further hydration results in the formation of the congruently melting R=3 [Zn(OH<sub>2</sub>)<sub>6</sub>][ZnCl<sub>4</sub>],  $T_{\rm m}=4.8$  °C (-3.0 for D<sub>2</sub>O). For this stoichiometric hydrate, the molecular ions and the corresponding CsCl-type molecular ion packing persist into the melt resulting in the formation of a room-temperature ionic liquid.

Two other low-temperature crystalline hydrates have been reported, at compositions R=2.5,  $[\mathrm{Zn}(\mathrm{OH}_2)_5][\mathrm{ZnCl}_4]$ , and 4.5,  $[\mathrm{Zn}(\mathrm{OH}_2)_6][\mathrm{ZnCl}_4] \cdot 3\mathrm{H}_2\mathrm{O}$ . However, no data supporting stoichiometric hydrates are observed between the R=1.33 and 3 hydrates. Thermodynamic DSC measurements (Figure S10) indicate normal eutectic behavior between 1.33 < R < 3, with the eutectic composition of R=2.4 at a eutectic temperature of -1 °C ( $\mathrm{H}_2\mathrm{O}$ ); -7 °C ( $\mathrm{D}_2\mathrm{O}$ ). This suggests that the R=2.5 crystalline hydrate, reported to be synthesized at 7 °C and a composition of 73 mol % water, and also reported in the original Mylius—Deitz phase diagram, is unlikely to be a pure zinc chloride hydrate. Instead, it is most likely a hydroxide/chloride impurity phase.

A lower-temperature eutectic is observed on the water-rich side of the R = 3 hydrate as seen by the decreasing liquidus temperature and constant eutectic transition in the DSC traces of Figure S10. This eutectic temperature is -32 °C for H<sub>2</sub>O and -37 °C for D<sub>2</sub>O. Lever rule analysis of the liquidus and eutectic peaks place this eutectic composition at about R = 4.1(80.4 mol % water). We have not been able to clearly establish the second crystalline phase for this eutectic, as essentially no crystallization was observed between this composition and R > 9, where ice is observed as the crystallizing phase. However, the liquidus of the first ice crystalizing composition is well below the -32 °C eutectic observed for the 4 > R > 3 compositions, suggesting the likelihood of an additional crystalline hydrate between the R = 3 and pure water. The asymmetry of the endothermic peak toward low temperature observed in the DSC for the R = 4.65 is also indicative of an additional crystalline phase; characteristic of a liquidus transition on the water-rich side of the  $R \sim 4.1$  eutectic. Furthermore, in our work measuring the rate of R = 3 hydrate crystal growth by polarized light microscopy as a function of added water  $(4.1 > R \ge 3)$ , we observe the growth of crystals with two distinct morphologies and distinct growth rates at temperatures below the -32 °C eutectic but crystals with only a single morphology above the eutectic (Figure S5). These data are consistent with the existence of the R = 4.5 hydrate, noted in the original Mylius-Deitz phase diagram, <sup>13</sup> and also crystallographically characterized by Hennings. 18 Because of the remaining uncertainty about this phase, it is indicated with a dashed line on the phase diagram, and the corresponding liquidus line is drawn in gray.

IV.I.III. Debye—Hückel Limiting and Extended Debye—Hückel Solutions (Hydrate Classes I and II). The water-rich side of the phase diagram, i.e., R > 4.5 is best described as a deep eutectic solvent. We find no evidence of the eutectic transition in DSC experiments down to -80 °C. The lowest liquidus transition we have observed was at -50 °C for the R = 7.9 composition (88.7 mol %  $H_2O$ ). No liquidus transition was

detectible in the R=6.9 (87.3 mol %) composition. However, Hennings et al. report growing a single crystal of the R=4.5 hydrate from an R=6.4 (86.6 mol %  $\rm H_2O$ ) composition at  $-50~\rm ^{\circ}C.^{18}$  These data suggest limits to define the eutectic composition to be between 87 and 88 mol %  $\rm H_2O$ . Estimating the liquidus curvature from the bounding compositions, we estimate the eutectic temperature to be at least below  $-60~\rm ^{\circ}C$ , substantially deeper than is observed for  $\rm CaCl_2$  at  $-51~\rm ^{\circ}C$  and 93.6 mol % water and comparable to potassium acetate, KOAc, observed at  $-60~\rm ^{\circ}C$  and 84.5 mol % water. <sup>55</sup>

IV.II. Crystalline Polymorphism of ZnCl<sub>2</sub>. Four crystalline polymorphs have been reported for ZnCl<sub>2</sub>, however, the interrelationship between them remains to be fully established. <sup>19–23</sup> Both kinetic and thermodynamic factors, including the presence of small amounts of water (<10 mol % or <2.7 wt %) result in substantial history dependence as to which phase(s) are observed. However, using the combination of *in situ* diffraction (Figures 1, 2, and S2), *ex situ* diffraction (Figures S3 and S4), gravimetric analysis (Figures 3 and S6), and DSC data (Figures S7 and S10–S12), we provide a comprehensive description of connections between phases by considering both the sorption of water into anhydrous ZnCl<sub>2</sub> and desorption from hydrate phases.

The  $\delta$ -phase of ZnCl<sub>2</sub> can be established as the only truly anhydrous thermodynamically stable form of ZnCl2, most effectively prepared by sublimation after heating above 350 °C to ensure removal of all water. As originally reported,<sup>21</sup> and observed by TtXRD (Figures 2 and 5), the  $\delta$ -phase can be prepared from the melt, but only remains stable to room temperature in the absence of all moisture. In situ diffraction measurements showed that the  $\beta$ -phase may nucleate out of the melt before subsequently transforming to the  $\delta$ -phase (see Figure 2; also observed by TtXRD with pure  $\delta$ -ZnCl<sub>2</sub>). As will be discussed below, the  $\beta$ -phase is the high-temperature gashydrate phase. While both  $\beta$ - and  $\delta$ -phases exhibit a hexagonal close-packed (hcp) type packing of the chloride sublattice, they exhibit distinct arrangements of the zinc cations. We propose that the  $\beta$ -phase zinc positions may be more closely related to the zinc distribution in the melt, similar to the behavior we previously described for the transformation of the kinetic  $\beta$ - to the thermodynamic  $\alpha$ -CuAlCl<sub>4</sub>. So

While no stoichiometric hydrate phases are identified between the pure anhydrous  $\delta$ -phase and the R = 1.33hydrate, the  $\alpha$ -,  $\beta$ -, and  $\gamma$ -phases are most likely Class V gashydrate phases. Upon exposure to small amounts of water vapor at room temperature, the  $\delta$ -phase converts to the  $\alpha$ phase (see Figure 1). The  $\alpha$ -phase also can be synthesized by sublimation of ZnCl<sub>2</sub> from lower temperatures under weaker vacuum where water vapor is not fully removed, 19,20,23 or by precipitation from saturated solutions. Alternatively, if  $\delta$ -ZnCl<sub>2</sub> is directly exposed to 1–30 mol % of liquid water, the  $\gamma$ -phase is observed (Figure S3a). The  $\gamma$ -phase also is reportedly obtained by cooling a boiling aqueous solution of ZnCl<sub>2</sub>. <sup>23</sup> If a sample of the  $\gamma$ -phase is melted and recrystallized in a closed container such that the sample is exposed to autogenous  $P_{\rm H_2O}$ on cooling, it forms the  $\alpha$ -phase (Figure S3c), as when gasphase water is added to the  $\delta$ -phase. Furthermore, crystals isolated from a saturated, room-temperature solution exhibit the  $\alpha$ -phase. These data suggest that both  $\alpha$ - and  $\gamma$ -ZnCl<sub>2</sub> are room-temperature, gas-hydrate phases. While the γ-phase may be kinetically stabilized, at ambient temperature,  $\alpha$ -ZnCl<sub>2</sub> is the thermodynamic phase.

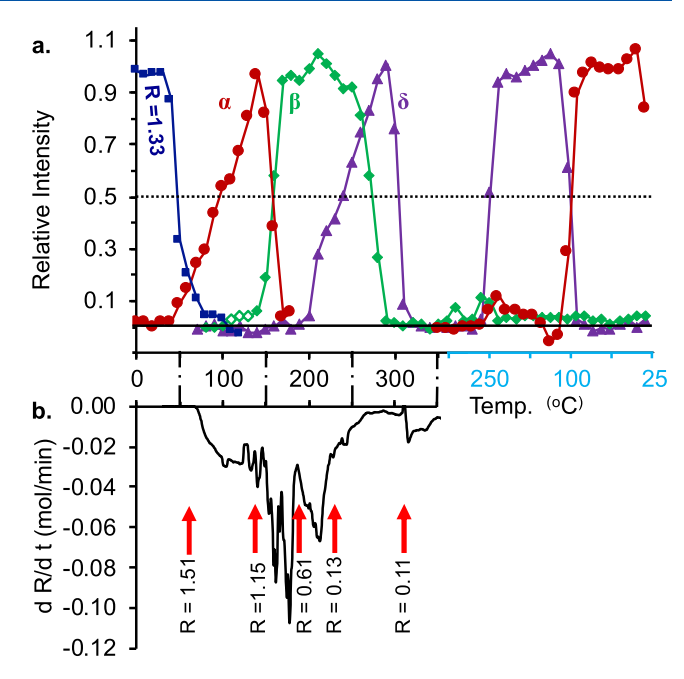


Figure 5. (a) Relative intensity of select diffraction peaks for ZnCl<sub>2</sub> polymorphs during the thermal decomposition of a hydrate slurry including the crystalline R=1.33 hydrate, and partial rehydration upon cooling under the autogenous  $P_{\rm H_2O}$  of the closed gas manifold; from the TtXRD experiment of Figure 2. R=1.33 hydrate, dark blue, (111) = 1.21 Å<sup>-1</sup>; α-ZnCl<sub>2</sub>, red, (123) = 3.17 Å<sup>-1</sup>, corrected with respect to overlapping peaks for the R=1.33, β and δ phases; β-ZnCl<sub>2</sub>, green, (111), (111), and (021)=1.23 Å<sup>-1</sup> (open green squares show the growth of the α-phase superstructure peak at 1.24 Å<sup>-1</sup>); δ-ZnCl<sub>2</sub>, purple, (111) = 1.64 Å<sup>-1</sup>. (b) First derivative of the thermal decomposition portion of the TGA trace Figure 4b. Molar water content at specific temperatures is indicated with red arrows.

To understand how both temperature and gas-hydrate water content control the polymorphism of ZnCl<sub>2</sub> it is useful to directly compare the TtXRD experiment of Figure 2 with the analogous TGA experiment of Figure 3b. Specifically, Figure 5 shows the relative appearance/disappearance of select diffraction peaks of each ZnCl<sub>2</sub> polymorph during the thermal dehydration of the 1.33 hydrate, compared to the first derivative of the thermal decomposition by TGA.

As the slurry-hydrate sample is heated, the  $\alpha$ -phase first appears commensurate with the onset of the loss of the crystalline 1.33 hydrate, around 60 °C. Notably, the crystalline 1.33 hydrate essentially disappears prior to the onset of water loss upon heating, and substantially precedes the full growth of  $\alpha$ -ZnCl<sub>2</sub>, with their relative intensities crossing at about 18%. These data demonstrate the upper-temperature limit of stability for the R=1.33 hydrate, above which the liquid and  $\alpha$ -phase are thermodynamically stable; the transition does not require water loss from the system.

The complete formation of  $\alpha$ -ZnCl<sub>2</sub> occurs concurrently with the loss of about 0.4 equiv of water from the R=1.5 slurry observed by TGA between 70 and 150 °C. This likely corresponds to the endotherm observed in the DSC at 106 °C, Figure S7 (the temperature range is narrower and higher for the DSC measurement because of the greater autogenous vapor pressure in the hermetically sealed pans). Notably, this transition occurs about  $10^{\circ}$  above the temperature at which the sealed capillary sample of the 55 mol % water system is observed to be fully liquid, consistent with this being a water-

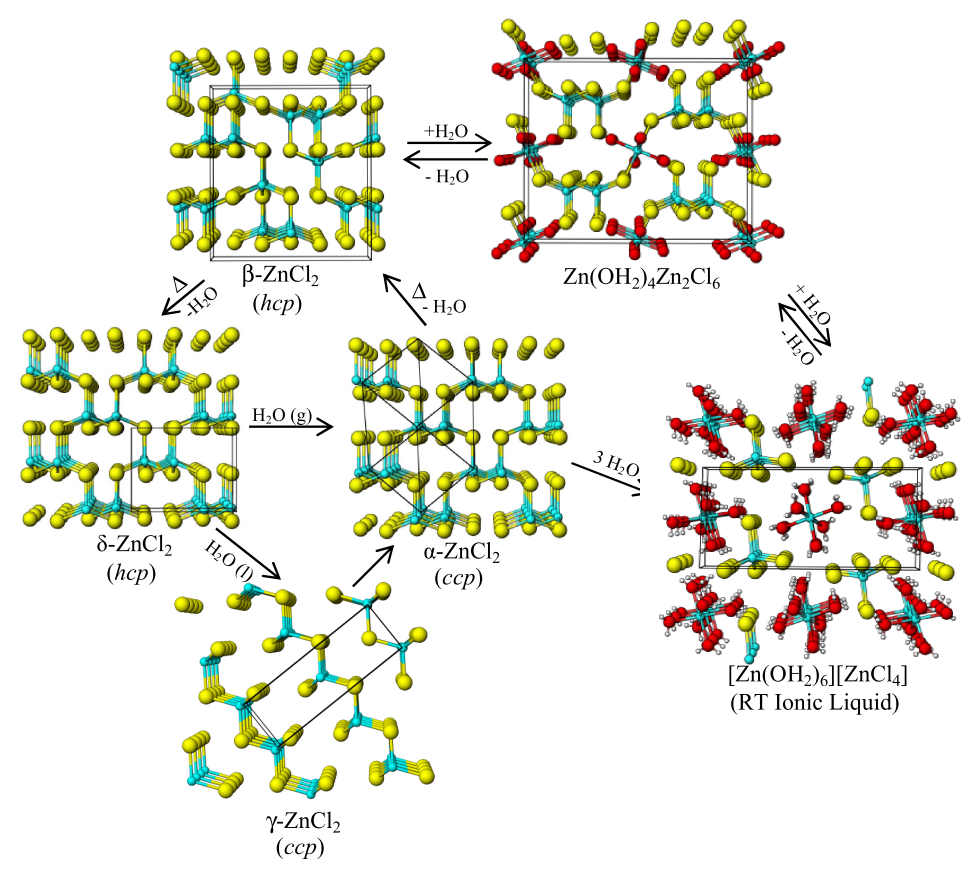


Figure 6. Schematic of the interrelationship between the  $\alpha$ ,  $\beta$ ,  $\delta$ , and  $\gamma$  phases of ZnCl<sub>2</sub>, as well as their relation to the first crystalline/ionic liquid hydrates. (Zn, turquoise; Cl, yellow; O, red; and H, white).

loss rather than a first-order structural transition. A complementary exothermic event at ~105 °C is observed by DSC upon cooling (Figure S7c), the temperature at which the  $\delta$ -phase converts back to the α-phase in the TtXRD (Figure 2), likely upon the resorption of water vapor. Under those cooling conditions, the relative intensity of the  $\delta$  and  $\alpha$  phases cross at 50%, consistent with an A  $\rightarrow$  B transition with no intermediates (Figure 5). The derivative weight-loss plot shows a more gradual onset of weight loss during the formation of  $\alpha$ -ZnCl<sub>2</sub> by thermal desorption from about 70 to 100 °C, followed by a near steady-state weight loss from 110 to 150 °C. The latter temperature range corresponds to the appearance of the possible  $\alpha$ -superstructure peak (open green squares in Figure 5a), and the increased slope of the thermal contraction of the c-lattice constant (Figure S1a). These data demonstrate that upon heating of hydrate solutions,  $\alpha$ -ZnCl<sub>2</sub> can form from the decomposition of the R = 1.33 hydrate, from the L  $\rightarrow \alpha$  transformation, or by water loss from the system. Further, they suggest that water is lost from both the solution and from the  $\alpha$ -gas-hydrate crystalline lattice. Because the conditions of water loss are significantly dependent on the  $P_{\mathrm{H,O}}$ , the temperature of this transition varies somewhat between techniques/reaction conditions, with a lower-temperature onset observed in the open TGA system compared to the sealed DSC cells. As such, this water-loss transition is represented as a dotted line on the phase diagram in Figure 4.

A subsequent loss of about 0.5 equiv of water, possibly in two event steps (Figure 5b), occurs between 150 and 180 °C during which the diffraction experiment reveals a complete transition from  $\alpha$ - to  $\beta$ -ZnCl<sub>2</sub>. The  $\alpha$ -phase does not

congruently melt but rather transforms to the  $\beta$ -phase upon heating (see Figure 2). The  $\beta$ -phase can kinetically exist at room temperature, formed by in vacuo dehydration of the 1.33 hydrate phase (Figure S2). The abrupt change in the intensity of several of the  $\beta$ -phase diffraction peaks starting around 110 °C in the in vacuo experiment is consistent with the sample physically moving at the onset of additional water loss. However, the  $\beta$ -phase appears to be thermodynamically stable with respect to the  $\alpha$ -phase above 150 °C, designated as the upper temperature of stability of the  $\alpha$ -phase on the phase diagram. The first of the two weight-loss peaks between 150 and 180 °C, observed in the first derivative plot, is directly coincident with the  $\alpha \to \beta$  transition (Figure 5). The second weight-loss peak with no significant change in the intensity of the  $\beta$ -phase is consistent with water loss from the  $\beta$ -gashydrate. The relative diffraction intensity for  $\alpha$ - vs  $\beta$ -ZnCl<sub>2</sub> across this temperature range crosses at 50%. This direct A  $\rightarrow$ B transformation suggests that the water loss between 150 and 180 °C is primarily from the gas-hydrate crystals rather than from any liquid phase, as a combined  $\alpha \to \beta$  plus L  $\to \beta$ process would exhibit crossing of the relative crystalline distributions above 50%. Notably, no discrete event is observed in the DSC corresponding to these transitions. This suggests a small enthalpic difference between the  $\alpha$  and  $\beta$  crystalline lattices, and further, that the water loss from  $\alpha$  and  $\beta$  crystalline gas hydrates is sufficiently small and gradual that it is observed as a decreasing baseline, rather than as a peak in the DSC.

An additional 0.5 equiv of water is lost between 190 and 250 °C, reaching a maximum rate at 213 °C, concurrent with the 212 °C endotherm frequently observed upon heating in the

DSC. This feature in the DSC appears even for the more water-rich 55 mol % water composition which is fully molten at a significantly lower temperature (Figure S8), indicating water loss from solution. The  $P_{H,O}$  also affects the temperature of this water-loss event, accounting for the difference between DSC and TGA measurements. By diffraction, the  $\beta \rightarrow \delta$  phase transition is observed to occur over a similarly wide temperature range, between 190 and 270 °C in the closed capillary system of the TtXRD experiment (Figure 2), and between 200 and 250 °C while heating under dynamic vacuum (Figure S2). Notably, no corresponding exotherm at 212 °C is observed in the cooling DSC traces, and neither is a  $\delta \rightarrow \beta$ transition ever observed by diffraction. Comparison of the TGA and TtXRD data (Figure 5) shows this water loss to coincide with an initial slight increase in the intensity of the  $\beta$ phase, consistent with some L  $\rightarrow \beta$  transformation preceding the first appearance of the  $\delta$ -phase. However, the crossing of the  $\beta$  and  $\delta$  diffraction peaks at about 75% relative intensity indicates that throughout this transition, water is lost from both the solution and the  $\beta$ -ZnCl<sub>2</sub> gas-hydrate to form  $\delta$ -ZnCl<sub>2</sub>. Notably, three phases (the solution liquid, and crystalline  $\beta$ -, and  $\delta$ -ZnCl<sub>2</sub>) coexist across this temperature region. The 50-80 °C temperature range over which this transition is observed suggests that the coexistence of these three phases is not a kinetic artifact. Instead, it is a result of the added variable of water vapor pressure in this nonisobaric system, which allows the coexistence of the three phases over a temperature-composition region as water is lost from both the solution and  $\beta$ -ZnCl<sub>2</sub> gas-hydrate to form  $\delta$ -ZnCl<sub>2</sub>. This transition is noted as a dot-dash line on the phase diagram.

Above 290 °C,  $\delta$ -ZnCl<sub>2</sub> is the only crystalline phase observed. When the temperature of the system crosses the liquidus between 300 and 310 °C, R = 0.1, or 10 mol % water, remains in the TGA sample. All other indications suggest that  $\delta$ -ZnCl<sub>2</sub> is truly anhydrous. Thus, we presume the water remaining above 275 °C and below the liquidus is associated with the liquid/solution phase. The last water of hydration is not lost from the system until above the 318 °C melting point of anhydrous  $\delta$ -ZnCl<sub>2</sub>.

It is worth noting that the phase heterogeneity and gradual phase transformations observed by diffraction and TGA likely account for some of the variation between heating and cooling cycles, and the frequent lack of distinct features in the DSC traces. Depending on the amounts and compositions of the respective phases, the  $1.33 \rightarrow \alpha$ , L  $\rightarrow \alpha$ ,  $\gamma \rightarrow \alpha$ ,  $\alpha \rightarrow \beta$ , L  $\rightarrow \beta$ , and  $\beta \rightarrow \delta$  transitions may be more or less apparent in the DSC. Furthermore, the hysteretic  $\alpha \rightarrow \beta \rightarrow \delta$  (heating) and  $\delta \rightarrow \alpha$  (cooling under exposure to small amounts of water vapor) suggest there is a significant kinetic barrier for  $\delta \rightarrow \beta$  gas solubility.

IV.III. Mechanistic Insight into the Hydration Process. Having considered the role of moisture in determining the  $ZnCl_2$  polymorphs, it is useful to evaluate the conditions under which the  $ZnCl_2: H_2O$  system forms both gas hydrates and stoichiometric crystalline hydrates to gain mechanistic insight to the hydration/dehydration process. The substantial hysteresis of crystalline hydrate formation suggests significant kinetic control over the reactivity.

A schematic summary of the structural interrelationships between the phases and their dependence on the presence of water is provided in Figure 6. Each crystalline polymorph of ZnCl<sub>2</sub> exhibits an approximate close packing of chloride anions

(ccp:  $\alpha$  and  $\gamma$ ; hcp:  $\beta$  and  $\delta$ ), with distinct distributions of the zinc cations into 1/4 of the corresponding tetrahedral interstices. The  $\alpha$ ,  $\beta$ , and  $\delta$  phases all exhibit three-dimensional (3D) network structures, whereas the  $\gamma$ -phase exhibits a two-dimensional (2D) layered structure. The direction of the reaction arrows in Figure 6 summarizes the sample history-dependent interrelationships.

The hydration hysteresis is dramatically apparent in the contrast between the conditions under which water will sorb into  $\operatorname{ZnCl}_2$  vs desorb from its hydrates. At 60 °C and above, we observed no water sorption into crystalline  $\delta$ - $\operatorname{ZnCl}_2$  when exposed to  $P_{\text{H}_2\text{O}} = 4.6$  Torr (Figure 3a). Below 60 °C, gravimetric sorption measurements at  $P_{\text{H}_2\text{O}} = 4.6$  Torr exhibit monotonic weight gain, with no inflections in the sorption curves to indicate the formation of intermediate hydrate phases prior to achieving the equilibrium sorption compositions of the hydrate melts (ionic liquids). At 57 °C, where sorption was first observed, the  $P_{\text{H}_2\text{O}} = 4.6$  Torr system equilibrated to an R = 1.7 composition (Figure 3a), with increasing water sorption as the temperature is reduced. However, when more water-rich ionic liquids are exposed to dry nitrogen at 31 °C, they dehydrate to an R = 1.5 composition (Figures 3b and S6).

Similar hydration hysteresis is observed in the in situ diffraction experiments (Figures 1, 2, and S2). After the initial  $\delta \rightarrow \alpha$  transition upon exposure to water vapor at room temperature, no other crystalline phases are observed prior to the formation of a hydrate melt other than some transient formation of  $\beta$ -ZnCl<sub>2</sub>. The water vapor-induced  $\delta \rightarrow \alpha$  phase transformation in ZnCl<sub>2</sub> likely proceeds by a mechanism similar to that described for the isostructural CuAlCl<sub>4</sub>, wherein exposure of  $\beta$ -CuAlCl<sub>4</sub> to trace amounts of ethylene induces a  $\beta \rightarrow \alpha$  transition,<sup>56</sup> but exposure to greater amounts of ethylene yields a mono- or di-ethylene adduct. 50 The  $\beta$ -CuAlCl<sub>4</sub> (structural analog to  $\delta$ -ZnCl<sub>2</sub>) transforms to  $\alpha$ -CuAlCl<sub>4</sub> (structural analog to  $\alpha$ -ZnCl<sub>2</sub>) by symmetry-allowed rotations of certain tetrahedra and intralayer self-diffusion of the Cu<sup>I</sup> cations. <sup>56</sup> By contrast, ex situ diffraction of samples of  $\delta$ -ZnCl<sub>2</sub> to which liquid H<sub>2</sub>O was added shows the initial formation of the  $\gamma$ -phase (Figure S2). These experimental conditions present distinct kinetic pathways for hydration. When exposed to only water vapor, there is a local excess of ZnCl<sub>2</sub> and the limiting reagent determining the kinetics is the water vapor. By contrast, when a droplet of liquid water is added to  $\delta$ -ZnCl<sub>2</sub>, there is an excess of water at the droplet-ZnCl<sub>2</sub> interface, making ZnCl<sub>2</sub> the limiting reagent. These contrasting kinetic conditions lead to the formation of the  $\alpha$ and  $\gamma$  gas-hydrate phases, respectively. The latter kinetic conditions, for which ZnCl<sub>2</sub> sees a local excess of water, result in the formation of the less ordered 2D network of  $\gamma$ -ZnCl<sub>2</sub> and yield a more heterogeneous material, with domains of higher and lower water contents. This heterogeneity is manifest in the irregular first DSC heat cycles (Figure S7a).

The formation and decomposition of the crystalline R=1.33 hydrate also significantly depends on sample history. It is most reliably synthesized by dehydrating a fully liquid sample with a composition of ~75 mol % water, but is not observed as an intermediate between anhydrous  $\delta$ -ZnCl<sub>2</sub> and the ionic liquid (Figure 1). However, upon incubation for about a week at room temperature in sealed vials, samples of  $\gamma$ -ZnCl<sub>2</sub> with ca. 10–30 mol % water did transform to a mixture of the R=1.33 hydrate and the  $\alpha$ -phase (Figure S3a). These data indicate that 1.33 crystalline hydrate formation upon direct water sorption is

possible but is restricted by a substantial activation barrier at least for the  $\delta$ ,  $\alpha$ , and  $\gamma$  polymorphs; an alternative reaction path leading to the higher hydrated ionic liquids is kinetically preferred.

This hysteretic sorption/desorption of water into ZnCl<sub>2</sub> contrasts with the directly reversible solid-state reconstruction of  $\alpha$ -CuAlCl<sub>4</sub> upon sorption/desorption of C<sub>2</sub>H<sub>4</sub><sup>50</sup> or CO,<sup>57</sup> particularly since  $\alpha$ -CuAlCl<sub>4</sub> is isostructural to  $\alpha$ -ZnCl<sub>2</sub>. In the α-CuAlCl<sub>4</sub> system, the C<sub>2</sub>H<sub>4</sub> or CO bind to the Cu<sup>I</sup> metal centers, and the resulting adduct structures possess an arrangement of metal chloride chains that can be directly traced to the parent phase. We propose the origin of the substantial activation barrier for direct gas to solid hydrate formation in ZnCl<sub>2</sub> is the lack of such a homologous Zn distribution between the parent  $\delta$ -,  $\alpha$ -, or  $\gamma$ -ZnCl<sub>2</sub> phases and the adduct R = 1.33 hydrate phase (see Figure 6). By contrast, cationic mobility in the ionic liquid compositions facilitates structural rearrangements necessary for the formation of the crystalline 1.33 hydrate structure upon water desorption. Interestingly, however, the structure of  $\beta$ -ZnCl<sub>2</sub> can be described as Zn[Zn<sub>2</sub>Cl<sub>6</sub>], i.e., with Zn<sup>2+</sup> cations linking  $[Zn_2Cl_6]^{2-}$  anionic chains. The perspective drawings in Figure 6 show the overall structural connectivity in the  $\beta$ -phase is homologous with that of the R = 1.33 hydrate structure, which can be described as  $[Zn(OH_2)_4][Zn_2Cl_6]$  where 1/3 of the Zn cations are partially hydrated by four water molecules and link corner-shared tetrahedral  $[Zn_2Cl_6]^{2-}$  anionic chains. This may explain why poorly crystalline  $\beta$ -ZnCl<sub>2</sub> is observed to directly form upon evacuation of the 1.33 hydrate at room temperature (Figure S2). Furthermore, if the reverse  $\beta \rightarrow 1.33$  hydrate formation is possible, then the transient appearance of a small amount of  $\beta$ -ZnCl<sub>2</sub> in the TtXRD sorption experiment of Figure 1 may reveal the reaction pathway to form the R = 1.33hydrate from an incubated sample of  $\alpha$ - or  $\gamma$ -ZnCl<sub>2</sub>, i.e.,  $\alpha \rightarrow \beta$  $\rightarrow$  1.33 or  $\gamma \rightarrow \alpha \rightarrow \beta \rightarrow$  1.33.

Evaluation of these crystalline structures demonstrates a hydration process that prioritizes tetrahedral Zn-Cl bonding over water coordination. Maximizing Zn-Cl bonding is further observed through a stepwise hydration process extending to higher hydration. While the R = 2.5 crystalline hydrate reported by Hennings et al. 18 does not appear on the phase diagram, likely a product resulting from a minor hydroxide impurity, it demonstrates an intermediate hydration pattern between that of the partially hydrated R = 1.33,  $[\text{Zn}(\text{OH}_2)_4]$ - $[Zn_2Cl_6]$ , <sup>14</sup> and fully hydrated R = 3,  $[Zn(OH_2)_6][ZnCl_4]$ . Its structure can be described as  $[Zn(OH_2)_5][ZnCl_4]$ , with half the Zn cations partially hydrated by five water molecules and bridged to  $[ZnCl_4]^{2-}$  anions. The crystal structure of the R =4.5 hydrate, better described as [Zn(OH<sub>2</sub>)<sub>6</sub>][ZnCl<sub>4</sub>]·3H<sub>2</sub>O, <sup>18</sup> shows that further hydration adds water to the lattice rather than dissociating additional Zn-Cl bonding. Raman measurements confirm that the  $[ZnCl_4]^{2-}$  anion persists in aqueous  $ZnCl_2$  solutions even to high dilution. As such, the significant covalency of the Zn-Cl bonding limits the extent to which the zinc cations are hydrated.

Because the R=3 hydrate is a congruently melting composition, evaluation of the magnitude of the melting/fusion transitions provides additional insight into crystalline hydrate formation. The heat of fusion for the R=3 hydrate is -13.7 kJ/mol for the hydrate (H<sub>2</sub>O) and -11.4 kJ/mol for the deuterate (D<sub>2</sub>O), indicative of stronger hydrogen- than deuterium-bonding. Since the composition of the congruent melt is equivalent on either side of the liquidus,  $\Delta S^{\circ}_{\rm fus}=$ 

 $\Delta H^{\circ}_{\text{fus}}/T_{\text{m}}$ . Thus,  $\Delta S^{\circ}_{\text{fus}}$  for the R=3 hydrates can be calculated: (H<sub>2</sub>O)  $-49.3 \text{ J/(mol \cdot K)}$  and (D<sub>2</sub>O)  $-42.2 \text{ J/(mol \cdot K)}$ K). The melting points, enthalpic and entropic parameters, demonstrate inverse thermodynamic H/D isotope effects with respect to that observed for pure water. On a per water molecule basis, the  $\Delta H^{\circ}_{fus}$  and  $\Delta S^{\circ}_{fus}$  of the R=3 hydrate is only about 2/3 the magnitude observed for pure water [ $H_2O$ :  $T_{\rm m} = 0.0~{\rm ^{\circ}C},~\Delta H^{\circ}_{\rm fus} = -6.006~{\rm kJ/mol},~\Delta S^{\circ}_{\rm fus} = -21.99~{\rm J/mol\cdot K};~D_2{\rm O}:~T_{\rm m} = 3.8~{\rm ^{\circ}C},~\Delta H^{\circ}_{\rm fus} = -6.132~{\rm kJ/mol},~\Delta S^{\circ}_{\rm fus} = -6.$ -22.13 J/(mol·K)], 58 indicative of a smaller difference between the liquid and crystalline forms of the R = 3 hydrate than between the liquid and crystalline forms of water. However, the magnitude of the thermodynamic H/D isotope effects is substantially larger for the R = 3 hydrate ( $\Delta H^{\circ}_{\text{fus H}}$ /  $\Delta H^{\circ}_{\text{fus D}} = 1.20$ ,  $\Delta S^{\circ}_{\text{fus H}}/\Delta S^{\circ}_{\text{fus D}} = 1.17$ ) than for pure water  $(\Delta H^{\circ}_{\text{fus H}}/\Delta H^{\circ}_{\text{fus D}} = 0.979$ ,  $\Delta S^{\circ}_{\text{fus H}}/\Delta S^{\circ}_{\text{fus D}} = 0.994$ ). This comparative isotope effect suggests that reorganization of hydrogen bonding is more important to the crystallization of the R = 3 hydrate than it is for ice crystallization.

For compositions more dilute than the most water-rich eutectic, i.e., greater than about 87 mol % water, one shifts into the regime where the phase diagram describes the influence of the solute on the water network, rather than the influence of the water as solvent acting on the solute. Here, it is interesting to note that the freezing point depression observed by adding ZnCl<sub>2</sub> to water significantly exceeds that expected based on a standard application of Blagden's law of freezing point depression. For example, solutions more concentrated than 0.3 m (99.8 mol % water) exhibit a freezing point that is 15 to 60% lower than would be expected for an aqueous salt solution dissociating into three ions. And because, as previously described, the [ZnCl<sub>4</sub>]<sup>2-</sup> anion persists at high-dilution ZnCl<sub>2</sub>, <sup>16,17</sup> the three-ion assumption for colligative properties is an overestimate of the actual solute concentration. By contrast, these data appear to be most consistent with much earlier descriptions of salt solutions<sup>59</sup> by Rüdorff<sup>60</sup> and de Coppet,<sup>61</sup> who suggested that the so-called waters of crystallization are integral parts of the dissolved substances. Water molecules strongly interacting with the solute cannot equivalently be considered part of the solvent, thus resulting in higher effective concentrations and correspondingly deeper freezing points. A more thorough analysis of the role of waters of hydration on the freezing of ice from the zinc chloride solutions will be presented in a subsequent manuscript.

Finally, despite the hysteretic sorption/desorption of water into  $ZnCl_2$ , it is important to note the reversibility of water (de)sorption, at least for the more  $ZnCl_2$ -rich compositions. Even under dynamic vacuum, we find no evidence of loss of HCl and subsequent formation of hydroxide impurities from concentrated solutions, a common, albeit little recognized problem in commercial  $ZnCl_2$  preparation. However, while we have not extensively evaluated the limiting synthetic conditions, for dilute solutions (e.g., >100 equiv of water), we regularly observe the formation of ~1 wt % basic zinc chloride impurity,  $Zn_5Cl_2(OH)_8\cdot H_2O$ , upon evaporating under heat and reduced pressure. This suggests that HCl loss leading to hydroxide formation only occurs from compositions on the water-rich side of the ice—R = 4.5 eutectic.

#### **V. CONCLUSIONS**

Systematic measurements by calorimetry, gravimetric analysis, and diffraction clearly establish the  $\delta$ -phase of ZnCl<sub>2</sub> to be the pure, anhydrous composition. Small amounts of water vapor

result in the transformation of this polymorph to the gashydrate α-ZnCl<sub>2</sub>. Alternatively, exposure of anhydrous δ-ZnCl<sub>2</sub> to small amounts of liquid water, i.e., providing a higher local concentration of water than is achieved by vapor-phase hydration, yields the kinetic product  $\gamma$ -ZnCl<sub>2</sub>. Upon partial dehydration,  $\alpha$ -ZnCl<sub>2</sub> is converted to the  $\beta$ -phase. An anhydrous form of the  $\beta$ -phase may be kinetically accessible just below  $T_{\rm m}$ , observed as a transient first-nucleating species from some melt experiments. The gas-hydrate form of  $\beta$ -ZnCl<sub>2</sub> appears to be the thermodynamically stable phase above the upper-temperature limit of  $\alpha$ -ZnCl<sub>2</sub> and below the limit for the anhydrous  $\delta$ -ZnCl<sub>2</sub>.  $\beta$ -ZnCl<sub>2</sub> can be kinetically stabilized by direct evacuation of the R = 1.33 hydrate because of the homology of the zinc chloride network in those two phases. The lowest-energy pathway to hydrate anhydrous ZnCl<sub>2</sub> first extracts molecular ions into an ionic liquid rather than being lattice-directed, which would have allowed for the direct formation of crystalline hydrates by water vapor sorption into the parent phase. However, a lattice-directed path to crystalline hydrate formation may uniquely exist from the metastable  $\beta$ phase. Dehydration of ionic liquid compositions leads to the formation of the R = 1.33 crystalline hydrate before gashydrate phases are formed. Remarkably, the last waters of hydration are not removed from ZnCl<sub>2</sub> until above the melting point of the pure phase.

Using the ultrapure, doubly sublimed  $\operatorname{ZnCl_2}$  to map the  $\operatorname{ZnCl_2}: \operatorname{H_2O}$  phase diagram establishes the existence of the crystalline hydrates with compositions R=1.33, 3, and 4.5. The other crystalline hydrate compositions reported in the historic literature are most likely phases resulting from some amounts of hydroxide impurities that are formed by loss of HCl from dilute solutions. The strong interaction between  $\operatorname{Zn^{2+}}$  and water makes the zinc-bound water a strong hydrogenbond donor, yielding an inverse thermodynamic H/D isotope effect with respect to pure water. Because of the strong interaction between  $\operatorname{ZnCl_2}$  and water, additional liquid hydrate interactions exist such that even in relatively dilute solutions, the amount of "solvent" water is less than expected, thus resulting in the  $\operatorname{ZnCl_2}: \operatorname{H_2O}$  system acting as a deep eutectic solvent.

The more accurate phase diagram, along with the systematic characterization of the interrelationship between gas-hydrate and stoichiometric hydrate phases presented in this work, provides invaluable insight for understanding the composition-dependent properties of salt brines. In addition, the structural homology between ZnCl<sub>2</sub> and SiO<sub>2</sub> has historically been of interest, <sup>62</sup> providing a low-temperature system with which to model complex crystalline and structural transitions. It is likely that the phase transformations of ZnCl<sub>2</sub> associated with different extents hydration described in this work suggest that the ZnCl<sub>2</sub>: H<sub>2</sub>O system can also be an invaluable low-temperature/low-pressure model system for better understanding the geologic role of water in the transformation of silicate structures.<sup>53</sup>

#### ASSOCIATED CONTENT

#### Supporting Information

The Supporting Information is available free of charge at https://pubs.acs.org/doi/10.1021/acs.jpcb.1c10530.

Detailed description of all results, including 12 additional data figures presenting diffraction, calorimetry, gravimetric, and photographic results (PDF)

#### AUTHOR INFORMATION

#### **Corresponding Author**

James D. Martin — Department of Chemistry, North Carolina State University, Raleigh, North Carolina 27695-8204, United States; orcid.org/0000-0001-7414-2683; Phone: 919-515-3402; Email: Jim\_Martin@ncsu.edu

#### **Authors**

Shelby B. Pillai – Department of Chemistry, North Carolina State University, Raleigh, North Carolina 27695-8204, United States

Robert J. Wilcox – Department of Chemistry, North Carolina State University, Raleigh, North Carolina 27695-8204, United States

Berkley G. Hillis – Department of Chemistry, North Carolina State University, Raleigh, North Carolina 27695-8204, United States

Bradley P. Losey – Department of Chemistry, North Carolina State University, Raleigh, North Carolina 27695-8204, United States

Complete contact information is available at: https://pubs.acs.org/10.1021/acs.jpcb.1c10530

#### Notes

The authors declare no competing financial interest.

#### ACKNOWLEDGMENTS

This work was supported by National Science Foundation via contracts DMR-0072828, 0305086, 0705190, 1709370, and 1950984, and ACS-PRF Grant 46439. Synchrotron diffraction experiments were conducted at the National Synchrotron Light Source, Brookhaven National Laboratory, supported by the division of materials sciences of the DOE, with assistance from Dr. Jonathan C. Hanson. Neutron diffraction experiments were conducted at the Spallation Neutron Source, sponsored by the Scientific User Facilities Division, Office of Basic Energy Sciences, U.S. Department of Energy (DOE), with assistance from Dr. Jöerg Neuefeind. Eric Gabilondo, Shaun O'Donnell, and Prof. Paul Maggard of NCSU are acknowledged for the collection of *ex situ* powder diffraction data.

#### **■** REFERENCES

- (1) Braunstein, J. Some aspects of solution chemistry in liquid mixtures of inorganic salts with water. *Inorg. Chim. Acta Rev.* **1968**, 2, 19–30
- (2) Baik, D.; Fray, D. Electrodeposition of zinc from high acid zinc chloride solutions. *J. Appl. Electrochem* **2001**, *31*, 1141–1147.
- (3) Beck, F.; Rüetschi, P. Rechargeable batteries with aqueous electrolytes. *Electrochim. Acta* **2000**, *45*, 2467–2482.
- (4) Marino, M.; Misuri, L.; Carati, A.; Brogioli, D. Proof-of-concept of a zinc-silver battery for the extraction of energy from a concentration difference. *Energies* **2014**, *7*, 3664–3683.
- (5) Zhang, Q.; Ma, Y.; Lu, Y.; Li, L.; Wan, F.; Zhang, K.; Chen, J. Modulating electrolyte structure for ultralow temperature aqueous zinc batteries. *Nat. Commun.* **2020**, *11*, No. 4463.
- (6) Jin, J.; Li, H.; Chen, C.; Zhang, B.; Xu, L.; Dong, B.; Song, H.; Dai, Q. Enhanced Performance of Perovskite Solar Cells with Zinc Chloride Additives. ACS Appl. Mater. Interfaces 2017, 9, 42875—42882
- (7) Barnes, H.; Rose, A. Origins of hydrothermal ores. *Science* **1998**, 279, 2064–2065.
- (8) Crerar, D.; Wood, S.; Brantley, S.; Bocarsly, A. Chemical controls on solubility of ore-forming minerals in hydrothermal solutions. *Can. Mineral.* **1985**, 23, 333–352.

- (9) Christianson, D. W. Structural biology of zinc. Adv. Protein Chem. 1991, 42, 281-355.
- (10) Prasad, A. S. Zinc: the biology and therapeutics of an ion. *Ann. Intern. Med.* 1996, 125, 142–143.
- (11) Jentsch, T. J.; Stein, V.; Weinreich, F.; Zdebik, A. A. Molecular structure and physiological function of chloride channels. *Physiol. Rev.* **2002**, *82*, 503–568.
- (12) Babich, H.; Stotzky, G. Toxicity of zinc to fungi, bacteria, and coliphages: influence of chloride ions. *Appl. Environ. Microbiol.* **1978**, 36, 906–914.
- (13) Mylius, F.; Dietz, R. Uber das Chlorzink. Z. Anorg. Chem. 1905, 44, 209–220.
- (14) Follner, H.; Brehler, B. Die Kristallstruktur des ZnCl2.4/3H2O. *Acta Crystallogr., Sect. B: Struct. Sci.* 1970, 26, 1679–1682.
- (15) Wilcox, R. J.; Losey, B. P.; Folmer, J. C. W.; Martin, J. D.; Zeller, M.; Sommer, R. Crystalline and Liquid Structure of Zinc Chloride Trihydrate: A Unique Ionic Liquid. *Inorg. Chem.* **2015**, *54*, 1109–1119.
- (16) Wilcox, R. J. Sorption to Dissolution: The Reactivity of Small Molecules with Condensed Phase Metal Halide Networks. Ph.D. Thesis, North Carolina State University, 2009.
- (17) Losey, B. P. Understanding Solvation: A Case Study in Zinc Chloride Dissolution. Ph.D. Thesis, North Carolina State University, 2018.
- (18) Hennings, E.; Schmidt, H.; Voigt, W. Crystal structures of ZnCl<sub>2</sub>·2.5H<sub>2</sub>O, ZnCl<sub>2</sub>·3H<sub>2</sub>O and ZnCl<sub>2</sub>·4.5H<sub>2</sub>O. Acta Crystallogr., Sect. E: Struct. Rep. Online **2014**, 70, 515–518.
- (19) Brehler, B. Über das  $\alpha$  und  $\beta$ -ZnCl<sub>2</sub>. Naturwissenschaften 1959, 46, No. 554.
- (20) Brehler, B. Kristallstrukturuntersuchungen an ZnCl<sub>2</sub>. Z. Kristallogr. **1961**, 115, 373–402.
- (21) Yakel, H. L.; Brynestad, J. Refinement of the Crystal Structure of Orthorhombic Zinc Chloride. *Inorg. Chem.* **1978**, *17*, 3294–3296.
- (22) Brynestad, J.; Yakel, H. L. Preparation and Synthesis of Anhydrous Zinc Chloride. *Inorg. Chem.* **1978**, *17*, 1376–1377.
- (23) Oswald, H. R.; Jaggi, H. Zur Struktur der wasserfreien Zinkhalogenide I. Die wasserfreien Zinkchloride. *Helv. Chim. Acta* **1960**, 43, 72–77.
- (24) Harris, A.; Parton, H. The transport numbers of zinc chloride from emf measurements. *Trans. Faraday Soc.* **1940**, *36*, 1139–1141.
- (25) Foxton, F.; Shutt, W. The activity of zinc chloride in concentrated solution. *Trans. Faraday Soc.* **1927**, 23, 480–488.
- (26) Robinson, R.; Stokes, R.; Wilson, J. M. A thermodynamic study of bivalent metal halides in aqueous solution. *Trans. Faraday Soc.* **1940**, *36*, 733–748.
- (27) Dunsmore, H. S.; Paterson, R. Re-determination of the standard electrode potential of zinc and mean molal activity coefficients for aqueous zinc chloride at 298.15 K. *J. Chem. Soc., Faraday Trans.* 1 1976, 72, 495–503.
- (28) Goldberg, R. N. Evaluated activity and osmotic coefficients for aqueous solutions: Bi-univalent compounds of zinc, cadmium, and ethylene bis (trimethylammonium) chloride and iodide. *J. Phys. Chem. Ref. Data* **1981**, *10*, 1–56.
- (29) Hittorf, W. Das Verhalten der Diaphragmen bei der Elektrolyse von Salzlösungen. Z. Phys. Chem. 1903, 43, 239–249.
- (30) Rabinowitsch, A. Über die anomale Dissoziation in wässerigen Lösungen. Z. Phys. Chem. 1921, 99, 338–360.
- (31) Mead, D. J.; Fuoss, R. M. Conductance and viscosity of concentrated solutions of calcium and zinc chlorides. *J. Phys. Chem. A* **1945**, 49, 480–482.
- (32) Easteal, A.; Sare, E.; Moynihan, C.; Angell, C. Glass-transition temperature, electrical conductance, viscosity, molar volume, refractive index, and proton magnetic resonance study of chlorozinc complexation in the system ZnCl<sub>2</sub> + LiCl + H<sub>2</sub>O. *J. Solution Chem.* 1974, 3, 807–821.
- (33) Agnew, A.; Paterson, R. Transport in aqueous solutions of group IIB metal salts at 298.15 K. Part 6.—Irreversible thermodynamic parameters for zinc chloride and verification of Onsager's

- reciprocal relationships. J. Chem. Soc., Faraday Trans. 1 1978, 74, 2896-2906.
- (34) Miller, D. G.; Rard, J. A. Generalized isothermal transport coefficients of ZnCl2-H2O at 25° C. *J. Mol. Liq.* **1992**, *52*, 145–179.
- (35) Thomas, B.; Fray, D. The conductivity of aqueous zinc chloride solutions. *J. Appl. Electrochem.* **1982**, *12*, 1–5.
- (36) Nakamura, Y.; Shimokawa, S.; Futamata, K.; Shimoji, M. NMR relaxation study of water molecules in concentrated zinc chloride solutions. *J. Chem. Phys.* **1982**, *77*, 3258–3262.
- (37) Angell, C.; Sare, E. Glass-Forming Composition Regions and Glass Transition Temperatures for Aqueous Electrolyte Solutions. *J. Chem. Phys.* **1970**, *52*, 1058–1068.
- (38) Kirilenko, I. Glass formation in the ZnCl<sub>2</sub>-H<sub>2</sub>O system. Russ. J. Inorg. Chem. **2013**, 58, 1183–1186.
- (39) Irish, D. E.; McCarroll, B.; Young, T. F. Raman Study of Zinc Chloride Solutions. *J. Chem. Phys.* **1963**, *39*, 3436–3444.
- (40) Dagnall, S. P.; Hague, D. N.; Towl, A. D. C. X-ray diffraction study of aqueous zinc(II) nitrate. *J. Chem. Soc., Faraday Trans.* 2 1982, 78, 2161–2167.
- (41) Kuzmin, A.; Obst, S.; Purans, J. X-ray absorption spectroscopy and molecular dynamics studies of hydration in aqueous solutions. *J. Phys.: Condens. Matter* **1997**, *9*, 10065–10078.
- (42) Pavlov, M.; Siegbahn, P. E.; Sandström, M. Hydration of beryllium, magnesium, calcium, and zinc ions using density functional theory. *J. Phys. Chem. A* **1998**, *102*, 219–228.
- (43) Rudolph, W. W.; Pye, C. C. Zinc (II) hydration in aqueous solution. A Raman spectroscopic investigation and an ab-initio molecular orbital study. *Phys. Chem. Chem. Phys.* **1999**, *1*, 4583–4593.
- (44) D'Angelo, P.; Barone, V.; Chillemi, G.; Sanna, N.; Meyer-Klaucke, W.; Pavel, N. V. Hydrogen and Higher Shell Contributions in Zn2+, Ni2+, and Co2+ Aqueous Solutions: An X-ray Absorption Fine Structure and Molecular Dynamics Study. *J. Am. Chem. Soc.* **2002**, *124*, 1958–1967.
- (45) Fatmi, M. Q.; Hofer, T. S.; Randolf, B. R.; Rode, B. M. An extended ab initio QM/MM MD approach to structure and dynamics of Zn (II) in aqueous solution. *J. Chem. Phys.* **2005**, 123, No. 054514.
- (46) Cauët, E.; Bogatko, S.; Weare, J. H.; Fulton, J. L.; Schenter, G. K.; Bylaska, E. J. Structure and dynamics of the hydration shells of the Zn<sup>2+</sup> ion from ab initio molecular dynamics and combined ab initio and classical molecular dynamics simulations. *J. Chem Phys.* **2010**, 132, No. 194502.
- (47) Bock, C. W.; Markham, G. D.; Katz, A. K.; Glusker, J. P. The arrangement of first-and second-shell water molecules around metal ions: effects of charge and size. *Theor. Chem. Acc.* **2006**, *115*, 100–112.
- (48) Mackenzie, J. D.; Murphy, W. K. Structure of Glass-Forming Halides. II. Liquid Zinc Chloride. *J. Chem. Phys.* **1960**, 33, 366–369.
- (49) Norby, P. Synchrotron Powder Diffraction using Imaging Plates: Crystal Structure Determination and Rietveld Refinement. *J. Appl. Crystallogr.* **1997**, *30*, 21–30.
- (50) Sullivan, R. M.; Liu, H.; Smith, D. S.; Hanson, J. C.; Osterhout, D.; Ciraolo, M.; Grey, C. P.; Martin, J. D. Sorptive Reconstruction of the CuAlCl<sub>4</sub> Framework upon Reversible Ethylene Binding. *J. Am. Chem. Soc.* **2003**, *125*, 11065–11079.
- (51) Neuefeind, J.; Feygenson, M.; Carruth, J.; Hoffmann, R.; Chipley, K. K. The Nanoscale Ordered Materials Diffractometer NOMAD at the Spallation Neutron Source SNS. *Nucl. Instrum. Methods Phys. Res., Sect. B* **2012**, 287, 68–75.
- (52) Bodnar, R. J. Introduction to Aqueous-Electrolyte Fluid Inclusions. In *Fluid Inclusions: Analysis and Interpretation*; Mineralogical Association of Canada, 2003; Vol. 32, pp 81–99.
- (53) Whitney, J. A. The origin of granite: The role and source of water in the evolution of granitic magmas. *Geol. Soc. Am.* **1988**, *100*, 1886–1897.
- (54) Smith, E. L.; Abbott, A. P.; Ryder, K. S. Deep Eutectic Solvents (DESs) and Their Applications. *Chem. Rev.* **2014**, *114*, 11060–11082.
- (55) Federal Highway Administration Report FHWA-RD-202, 1996. https://www.fhwa.dot.gov/publications/research/safety/95202/005. cfm (accessed January 23, 2022).

- (56) Liu, H.; Sullivan, R. M.; Hanson, J. C.; Grey, C. P.; Martin, J. D. Kinetics and Mechanism of the  $\beta$  to  $\alpha$ -CuAlCl<sub>4</sub> Phase Transition: A Time Resolved <sup>63</sup>Cu MAS-NMR and Powder Diffraction Study. *J. Am. Chem. Soc.* **2001**, *123*, 7564–7573.
- (57) Capracotta, M. D.; Sullivan, R. M.; Martin, J. D. Sorptive Reconstruction of CuMCl<sub>4</sub> (M = Al and Ga) Upon Small Molecule Binding and The Competitive Binding of CO and Ethylene. *J. Am. Chem. Soc.* **2006**, *128*, 13463–13473.
- (58) Water Properties (Including Isotopologues). http://www.idc-online.com/technical\_references/pdfs/chemical\_engineering/Water\_properties.pdf (accessed January 23, 2022).
- (59) Reif-Acherman, S. The Pre-history of Cryoscopy: what was done before Raoult? Quim. Nova 2009, 32, 1677–1684.
- (60) Rüdorff, F. Über das Gefrieren des Wassers aus Salzlösungen. Ann. Phys. Chem. 1861, 190, 63-81.
- (61) De Coppet, L. C. Recherches sur la temperature de congelation des dissolutions salines. *Ann. Chim. Phys.* **1872**, *26*, 98–121.
- (62) Martin, J. D.; Dattelbaum, A. M.; Thornton, T. A.; Sullivan, R. M.; Yang, J.; Peachey, M. T. Metal Halide Analogues of Chalcogenides: a Building Block Approach to the Rational Synthesis of Solid-State Materials. *Chem. Mater.* **1998**, *10*, 2699–2713.

### ☐ Recommended by ACS

# On the Role of Water in the Formation of a Deep Eutectic Solvent Based on NiCl<sub>2</sub>·6H<sub>2</sub>O and Urea

Matteo Busato, Paola D'Angelo, et al.

MAY 26, 2022

INORGANIC CHEMISTRY

READ 🗹

## In Situ Determination of Speciation and Local Structure of NaCl-SrCl, and LiF-ZrF<sub>4</sub> Molten Salts

Timothy J. Lynch, Wilson K. S. Chiu, et al.

FEBRUARY 09, 2022

THE JOURNAL OF PHYSICAL CHEMISTRY B

READ 🗹

### Hydroxyethyl Group Effect on Properties of Bis[(trifluoromethyl)sulfonyl]imide-Type Ionic Liquids

Qingshan Liu, Ying Zang, et al.

SEPTEMBER 08, 2020

JOURNAL OF CHEMICAL & ENGINEERING DATA

READ 🗹

#### Dynamics of Ion Pairing in Dilute Aqueous HCl Solutions by Spectroscopic Measurements of Hydroxyl Radical Conversion into Dichloride Radical Anions

Lukasz Kazmierczak, Dorota Swiatla-Wojcik, et al.

AUGUST 12, 2021

THE JOURNAL OF PHYSICAL CHEMISTRY B

READ 🗹

Get More Suggestions >